

J.H. van der Sloot
Fokker - CB-SC/SO
Schiphol-Oost
The Netherlands

Summary

The 'Experimental Method Fokker', devised in 1956⁽¹⁾, is a computational procedure to estimate critical loads of stringer-stiffened panels, loaded in compression. Its main features are the inclusion in the formulation of the buckling condition the stiffness reduction effects due to local buckling and plasticity. The paper describes the generalization of the original Euler-Column mode formulations to account for a wide variety of buckling mode configurations in the panel lateral-direction. This generalization is accomplished by adopting a finite element method to effect the required integrations of the energy functional, defined for uniform panel end-shortening. The finite element procedure is also known as finite strip method.

The experimental character of the method is expressed by deriving the appropriate stiffness-reduction factors from test data to define a modified Ramberg-Osgood stress-strain law representation for typical panel elements. The original ideas of the E.M.F. are briefly outlined. The modifications, to generalize the existing procedures are summarized and computational results are compared with analytical solutions and correlated with test results.

I. Introduction

The determination of the critical load of stringer-stiffened panels in compression is still a complex computational problem, despite the availability of sophisticated computer systems. Since modern aerospace structural systems require highly efficient designs with respect to load carrying capacity against low specific weight, the general instability problem must be formulated to include such effects that arise from applying small geometric dimensions. Notably, thin skin- and stringer thicknesses may give rise to deformation patterns that are accompanied with local stress concentrations at lower load levels. The high stress/specific weight ratio required implies the circumstance that material points will be stressed into the plastic range of the material's stress-strain relationship. The requirement of minimum weight - hence small thickness dimensions - may induce the possibility of local buckling modes to develop at much lower load levels than the actual collapse load. Hence the problem of estimating the maximum load carrying capacity of stiffened panels in compression should include both effects of geometric non-linearity and stress disproportionality with strain. An analytical approach to solve the problem must, unfortunately, be precluded, apart from analyses performed on the basis of very simplified models. A complete numerical approach employing any modern descriptive technique, such as finite element or finite difference methods, to solve the stability problem is - in principle - possible,

utilizing existing computer codes, e.g. as reported in ref. 18, though considered non-practical from a designers' point of view.

The inherently time-consuming computations offer no efficient tool to consider and design optimum structural configurations, within the framework of the many parameters involved.

In view of the above considerations a method, devised to estimate critical panel-loads, accounting for both non-linear characteristics and being computationally efficient is offered by the E.M.F. The original formulation, developed in the early fifties, appeared in ref. 1. This historical setting should be appreciated with respect to the then available computational facilities.

Based upon the famous Euler column buckling formula, the method estimates the critical load for general instability, computed with appropriate stiffness reduction factors, arising from local buckling and/or plasticity effects.

The reduction factors are determined from a modified Ramberg-Osgood material-law representation. The modification consists of appending the polynomial expression with terms, the coefficients of which should represent stiffness reduction due to local buckling. This implies that the material-law is assumed to be valid for the locally buckled elements of the panel. This assumption removes the requirement of having to compute local quantities and the method may be looked at as an averaging procedure.

The experimental character of the method consists of the determination of the coefficients of the additional terms in the modified material-law from experiments.

Load-shortening curves, obtained from tests, for a wide variety of column geometries, served to fit the coefficients for a family of parametrized non-dimensional stress-strain-relations.

Some details will be outlined in the next section. The computational procedure, to determine the critical state of the panel, solves an eigenvalue problem, for which the modified material-law furnishes the stiffness coefficients, as a function of the panel end-shortening.

This eigenvalue problem, or buckling condition, arises from the observation, that the limit-point buckling form of the load-end-shortening curve as obtained from test panels, is indicative for bifurcation buckling for the model with a linear pre-buckling state. Incorporation of local buckling effects through modification of the material-law, allows the computation to pass the local buckling critical points of the load-deflection curve.

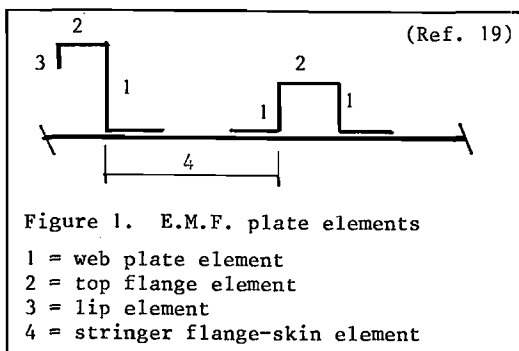
As indicated above the original formulation of the E.M.F. employs Euler's column buckling formula. Since that formulation assumes no panel section deformation nor shear deformability, it was considered recommendable to remove these assumptions from the earlier definitions so as to enlarge the range of panel geometries to be analysed with the E.M.F. For instance, compression panels stiffened with relatively heavy Z-stringers do show

considerable section deformation in the test. Hence, it may be assumed that the overall buckling mode exhibits such displacement components to initiate a torsional type of deformation of the panel cross-section. This type of behavior is represented in the model description through employing a discretization procedure in panel lateral direction, thereby maintaining the sinusoidal character of the overall buckling mode in axial direction. This approach, in conjunction with the E.M.F. procedures for stiffness reduction, allows the energy functional to be integrated in axial direction. In panel lateral direction this is accomplished approximately. The discretization method employed is of finite element type. The sinusoidal character of the longitudinal part of the displacement components, adopted herein, puts the method among the so-called finite strip⁽²⁾ approaches in finite element analysis.

In addition to the above generalization of the E.M.F. computational procedure, the present formulations include a typical bond-layer model and a rivet-line model to increase the methods' modelling capabilities. The next section summarizes the pertinent procedures employed in the E.M.F. to account for stiffness reduction due to local buckling and/or plasticity effects. Then the finite strip version is briefly discussed. For the derivation the incremental virtual work expression is utilized⁽²²⁾, in conjunction with a deformation type theory of plasticity⁽⁹⁾. As reported in a.o. refs. 8, 9 and 23, deformation theory better predicts test values and thus would appear to be well-suited for the formulation of the buckling condition in the E.M.F. In section III some recently obtained results are reported. Detailed information required for clarification of the formulations in section II are given in the appendix.

II. 1. Problem formulation

The typical features formulated in the E.M.F. for the determination of the stiffness reduction factors are fully outlined in a.o.: refs. 1, 3 and 12. A summary starts out by envisaging the panel to consist of plate elements, bounded by the panels' geometric layout, as indicated in fig.1.



It is noted that all elements are assumed prismatic in panel longitudinal direction. The elements are considered separately and for each a modified stress-strain relationship is determined to define its shortening behavior under a compressive load. Introducing the non-dimensional quantities for

stress and strain:

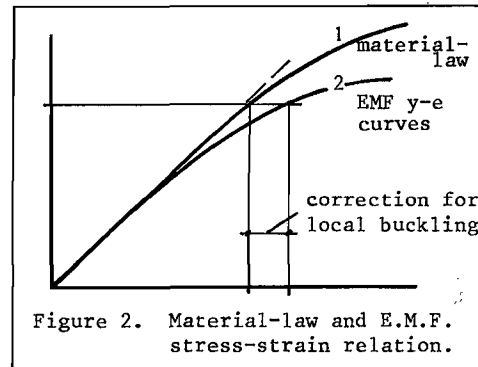
$$Y = \frac{\sigma}{\sigma_{0,2}}, \quad e = \epsilon \frac{E}{\sigma_{0,2}} \quad (1)$$

where: σ = uniaxial stress component, ϵ = the corresponding strain, E = Young's modulus and $\sigma_{0,2}$ = .2% yield stress, the material-law can be written as: ⁽³⁾ $e = Y + Q \cdot Y^n$. (2)

This expression is the non-dimensionalized form of the stress-strain relation given by Ramberg and Osgood⁽⁷⁾.

The constant Q is equal to $.002 E/\sigma_{0,2}$ (3)

The main assumption in the E.M.F. is depicted in figure 2.



It shows the modification of (2) to include the local buckling effect on the axial stiffness of the panel element under consideration and is expressed as follows:

$$e = Y + Q \cdot Y^n + R e^m \quad (4)$$

Since the panel consists of an aggregate of elements it is of advantage to parametrize the curve (4) to hold for various geometries represented by the constants R and m . The parameter to introduce is afforded by the so called effective width theory of von Karman for flat plates. It expresses the effective width of the plate as a function of the average-stress. The maximum edge stress of the plate element can be given by:

$$\sigma_E = K E (t/b_E)^2 \quad (5)$$

$$\text{or } b_E = f(\sigma_E)$$

where b_E denotes the effective width of the panel, and K is the local buckling stress coefficient, and t the plate thickness. By definition the local buckling stress expression is:

$$\sigma_L = K E \left(\frac{t}{b}\right)^2 \quad (6)$$

Hence, combining (5) and (6) yields

$$b_E/b = \sqrt{\frac{\sigma_L}{\sigma_E}} \quad (7)$$

with $b_E \cdot \sigma_E = b \cdot \sigma$, one finds:

$$\frac{\sigma}{\sigma_E} = \frac{b_E}{b} = \sqrt{\frac{\sigma_L}{\sigma_E}} \quad (8)$$

Introducing the material's yield stress $\sigma_{0,2}$, it follows that:

$$\sigma / \sigma_{0,2} = Y = f\left(\sqrt{\sigma_L / \sigma_{0,2}}\right) \quad (9)$$

or with: $X = \sqrt{\sigma_{0,2} / \sigma_L}$, (10)

(9) becomes $Y = f(X)$ and hence:

$$\bar{Y} = f(X), \quad (11)$$

where the overbar denotes maximum panel element stress. An extensive account of the above derivations can be found in a.o. ref. 4 and 5. The most important result is expression (11). As mentioned in the introduction many tests were carried out to establish the form of equation (11). A summary of test data considered is given in ref. 6. Next to Y , the corresponding value of the strain follows from these test results. Hence the coefficients R and m in equation (4) can be considered as

$$R = R(X), \quad m = m(x) \quad (12)$$

A typical curve of the form of equation (11) is given in figure 3.

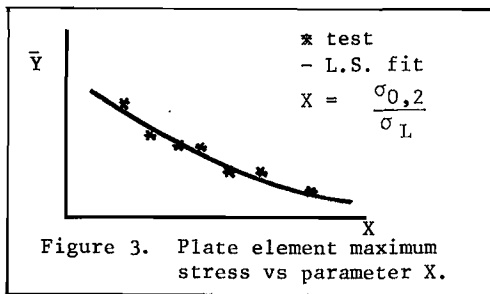


Figure 3. Plate element maximum stress vs parameter X.

A least square fit of the test results furnishes the analytical expression for equation (11), to be employed in the computations. The panel's critical load now follows from Eulers formula:

$$P_{cr} = \frac{\pi^2 EI}{L^2}, \quad (13)$$

in the following fashion:

- a. At preselected end-shortenings e , the overall section properties are calculated, with $E = E_t =$ tangent modulus from the set of appropriate curves contained in equation 4, to give the section centroid and moment of inertia.
- b. From 4, there also follows the total load from summing $y(e)$ for all plate elements.
- c. With a and b the length follows from (13):

$$L(e) = \pi \sqrt{\frac{\sum (E(e) * I(e))}{\sum P(e)}} \quad (14)$$

where the sum Σ extends over all elements.

- d. Varying e will give the length L corresponding to the length of the panel under consideration. Then the critical load is also known.

The generalization of the E.M.F. consists of recasting the buckling problem within the context of an energy formulation. To that effect the pertinent virtual work terms are constructed for a single plate element, and expressed in terms of displacement functions containing a set of free

amplitudes. Adding all terms relevant to the complete structural configuration, yields the system of equations for the amplitudes. Since this study strictly deals with the buckling problem the above mentioned procedure leads to considering the vanishing of the virtual work expression for the buckling displacements. This then yields a standard eigenvalue problem that computes the critical value of the panel end-shortening and determines the free amplitudes as the elements of the buckling mode.

The formulation starts out by selecting the strain displacement equations. In view of the general plate-element assemblies to consider, the proper choice for plate-element midplane-strains is:

$$\begin{aligned} \epsilon_x &= u_{,x} + \frac{1}{2} (u^2_{,x} + v^2_{,x} + w^2_{,x}) \\ \epsilon_y &= v_{,y} + \frac{1}{2} (u^2_{,y} + v^2_{,y} + w^2_{,y}) \end{aligned} \quad (15)$$

$$\gamma_{xy} = u_{,y} + v_{,x} + u_{,x}u_{,y} + v_{,x}v_{,y} + w_{,x}w_{,y}$$

where u, v are the axial- and lateral displacement functions of a plate element and w represents its deflection function. (see fig. 4). Here and in the following $_{,x}$ and $_{,y}$ denotes partial differentiation with respect to x and y respectively.

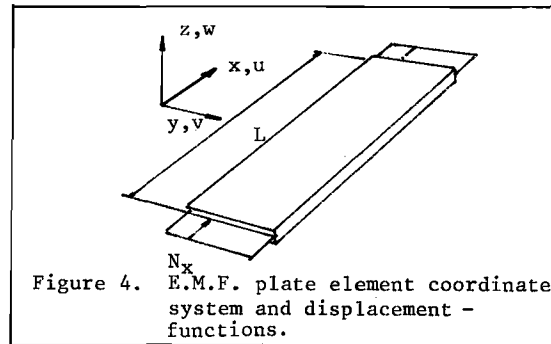


Figure 4. E.M.F. plate element coordinate system and displacement - functions.

The curvature expressions, relating the plate bending deformations to the deflection function w , may be taken as in standard plate theory, ref. 14, and 22,

$$\begin{aligned} \kappa_x &= -w_{,xx} \\ \kappa_y &= -w_{,yy} \\ \kappa_{xy} &= -w_{,xy} \end{aligned} \quad (16)$$

As indicated above the E.M.F. employs a modified stress-strain law to represent local buckling effects. A deformation type theory of plasticity is adopted to formulate the stress-strain relations for the individual plate elements. As outlined earlier, these constitutive relations are parametrized by the parameter X of equation (10). In general, see for instance refs. 8, 9, the incremental stress-strain relation for plate or shell type structures, with a generalized plane stress assumption, reads

$$\begin{aligned} \sigma_x &= E(A\epsilon_x + C\epsilon_y) \\ \sigma_y &= E(C\epsilon_x + D\epsilon_y) \\ \tau_{xy} &= EF\gamma_{xy} \end{aligned} \quad (17)$$

From ref. 9, with σ_x assumed to be the single non zero stress component in the pre-buckling state, the coefficients in equations 17 are,

$$\begin{aligned} A &= (1 + 3 ET/ES)/N \\ C &= (2 - 2(1-2\nu)ET/E)/N \\ D &= 4/N \\ F &= 1/2(1+\nu+3(E/ES-1)/2) \\ N &= 2-4\nu+3E/ES-(1-2\nu)^2Et/E \end{aligned} \quad (18)$$

where E = Young's modulus, E_t and E_s the tangent and secant modulus respectively and ν = poisson's ratio. The form of the virtual work expression, adopted for the present analysis reads (22,23)

$$\begin{aligned} \sum_i \int t \{ \sigma_x \delta \epsilon_x + \sigma_y \delta \epsilon_y + \tau_{xy} \delta \gamma_{xy} \} dx dy + \\ \sum_i \int \{ M_x \delta \kappa_x + M_y \delta \kappa_y + 2.M_{xy} \delta \kappa_{xy} \} dx dy + \\ \sum_i \int \sigma_x^0 (u_{,x} \delta u_{,x} + v_{,x} \delta v_{,x} + w_{,x} \delta w_{,x}) dx dy = 0. \end{aligned} \quad (19)$$

In equation 19, M_x , M_y and M_{xy} are the plate bending stress resultants defined by $M = \int \sigma_x z dz$ etc., δ denotes variational increment and the sum over i extends over all panel elements. The integrals in 19 are to be evaluated over the element's area. The last term in equation 19 follows from the main assumption of a linear pre-buckling state, characterized by the single stress component σ_x^0 . With utilization of equations 15, 16 and 17, condition 19 may be transformed to

$$\begin{aligned} \sum_i \int \{ t E f (A u_{,x} \delta u_{,x} + C v_{,y} \delta v_{,y} + C u_{,x} \delta v_{,y} + D v_{,y} \delta v_{,y} + \\ F (u_{,y} \delta u_{,y} + u_{,y} \delta v_{,x} + v_{,x} \delta u_{,y} + v_{,x} \delta v_{,x}) + \\ \frac{t}{12} (A w_{,xx} \delta w_{,xx} + C w_{,yy} \delta w_{,yy} + C w_{,xx} \delta w_{,yy} + D w_{,yy} \delta w_{,yy} + \\ 4 F w_{,xy} \delta w_{,xy}) + \\ \sigma_x^0 (u_{,x} \delta u_{,x} + v_{,x} \delta v_{,x} + w_{,x} \delta w_{,x}) \} dx dy = 0. \end{aligned} \quad (20)$$

In the derivation of equation 20, higher order terms than quadratic in the incremental displacement fields have been omitted, to arrive at the bifurcation eigenvalue problem contained in expression 20 for the critical stress. Then, for an assemblage of elements the appropriate expression for the critical state is obtained from the buckling condition, defined for uniform panel end-shortening, to ensure satisfaction of the plate elements' compatibility conditions. The relevant stress terms follow from the elements' material law, as is the case for the moduli contained in the coefficients A , C , D and F appearing in equation 20.

II. 2. Finite element development

The expression of equation 20 is now particularized for an application in finite element sense, on the basis of assuming specific coordinate functions for the buckling displacement fields u , v and w .

The typical character of the buckling problem allows to assume a particular choice for u , v and w in the form of product functions, such that

$$\begin{aligned} u &= U(y) * T_u(x) \\ v &= V(y) * T_v(x) \\ w &= W(y) * T_w(x) \end{aligned} \quad (21)$$

In (21) the factors $T(x)$ are chosen as trigonometric functions of the axial coordinate, anticipating the buckling wave form as observed in tests. For the present application the following table lists the functions $T(x)$ for both simply supported and clamped loaded edges.

	Si.Su.	Clamped
T_u	$\text{COS} \mu x$	$\text{SIN} \frac{2\pi x}{L}$
T_v	$\text{SIN} \mu x$	$1 - \text{COS} \frac{2\pi x}{L}$
T_w	$\text{SIN} \mu s$	$1 - \text{COS} \frac{2\pi x}{L}$

$$\mu = \frac{M\pi}{L}$$

M = wave number

Table 1.

These functions assure interelement compatibility as required for the variational condition employed. It is noted that the functions $T(x)$ for the simple support boundary conditions along the loaded edges presume a periodic buckling wave-form. The clamped-edge $T(x)$ -functions represent periodicity with a double axial wave length. In addition, the clamped edge functions should only be appreciated as a first approximation for the displacement field in view of the fact that these functions do not satisfy the equilibrium differential equations.

Substitution of the functions $T(x)$ into equation (20) permits direct integration along x of all separate terms. The factors $U(y)$, $V(y)$ and $W(y)$ in (21) are chosen to be simple polynomial expressions in the coordinate y of the particular element under consideration with $\eta = y/B_i$, in which B_i = width of i^{th} element:

$$\begin{aligned} U^i(\eta) &= U_1^i(1-\eta) + U_2^i\eta \\ V^i(\eta) &= V_1^i(1-\eta) + V_2^i\eta \\ W^i(\eta) &= W_1^i(2\eta^3 - 3\eta^2 + 1) + B_i \phi_1^i(-\eta^3 + 2\eta^2 - \eta) \\ &\quad + W_2^i(-2\eta^3 + 3\eta^2) + B_i \phi_2^i(-\eta^3 + \eta^2) \end{aligned} \quad (22)$$

Here U_p^i , V_p^i , W_p^i and ϕ_p^i are nodal amplitudes defined at the nodal points of the element edges $\eta = 0$ then $p = 1$ and for $\eta = 1$, $p = 2$, at $x = 0$ or $L/2$ on account of the particular choice of the functions $T(x)$ for u , v and w . Substitution of expressions (22) into equation (20) allows the integrations over y (or η) to be carried out. The final result then reads: (omitting subscript i)

$$\begin{aligned}
& \frac{1}{2} E \frac{t}{B} \left\{ \langle \frac{1}{4} \rangle \beta^2 U^t |N| \delta U + C \beta \langle \frac{1}{2} \rangle \{ U^t |D| \delta U + U^t |D^t| \delta U \} \right. \\
& + D \langle \frac{1}{3} \rangle U^t |F| \delta U + F \langle \frac{1}{1} \rangle U^t |F| \delta U + \\
& + \beta F \langle \frac{1}{2} \rangle U^t |D| \delta U + U^t |D^t| \delta U \} + \beta^2 F \langle \frac{1}{4} \rangle U^t |N| \delta U + \\
& \frac{t^2}{12 B^2} \left\{ A \beta^4 \langle \frac{1}{16} \rangle W^t |M| \delta W + \beta^2 C \langle \frac{1}{4} \rangle W^t |L+L^t| \delta W + \right. \\
& D \langle \frac{1}{3} \rangle W^t |K| \delta W + 4 F \beta^2 \langle \frac{1}{4} \rangle W^t |G| \delta W \} \\
& + \sigma_{XB}^0 t \left(\beta^2 \langle \frac{1}{4} \rangle U^t |N| \delta U + \beta^2 \langle \frac{1}{4} \rangle U^t |N| \delta U + \beta^2 \langle \frac{1}{4} \rangle W^t |M| \delta W \right) = 0.
\end{aligned} \tag{23}$$

Where: $\beta = \frac{M\pi B}{L}$, B = element width, L = element length, $\langle \frac{a}{b} \rangle$ is introduced as a concise notation for $\frac{a}{b}$ = simple support and b = clamped loaded edge boundary conditions. In addition | - | denotes matrix and $\bar{\sim}$ denotes vector, in particular

$$U^T = (U_1, U_2) \quad V^T = (V_1, V_2) \text{ and}$$

$$W^T = (W_1, \phi_1, W_2, \phi_2), \text{ where superscript T}$$

indicates transpose. The explicit matrix expressions are given in appendix I.

Equation 23 provides the stiffness matrices for the plate element. Consistent transformation with respect to the global coordinate system afford these matrices to apply for typical panel components such as webs and flanges.

Bondlayer and rivet-line models

In actual compression panel configurations the stringers are usually bonded or riveted to the skin. Since bondlayer behavior is of interest in the present investigation a model is adopted to simulate bond material mechanical behavior. The bonded joint's load carrying capability is described - in general - by a complex system of differential equations. In view of practical circumstances, that show much scatter to exist in mechanical properties and geometric parameters, it is deemed adequate for the analysis herein to adopt a simplified model to incorporate the essential features of bondlayer behavior in the buckling problem. Thus the strain-displacement relations proposed by Mayers and Durlinsky⁽¹⁰⁾ are employed. The variation of the strains in thickness direction is eliminated by averaging and the relevant relations are:

$$\begin{aligned}
\gamma_{xz} &= \frac{1}{t_b} (u_2 - u_1 + \frac{1}{2}(t_1 + t_b)w_{1,x} + \frac{1}{2}(t_2 + t_b)w_{2,x}). \\
\gamma_{yz} &= \frac{1}{t_b} (v_2 - v_1 + \frac{1}{2}(t_1 + t_b)w_{1,y} + \frac{1}{2}(t_2 + t_b)w_{2,y}). \\
\epsilon_z &= \frac{1}{t_b} (w_2 - w_1).
\end{aligned} \tag{24}$$

Here the subscripts 1,2 denote lower and upper adherent plates, see fig. 5.

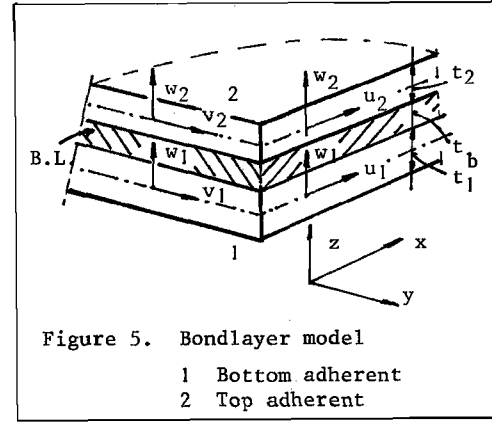


Figure 5. Bondlayer model

- 1 Bottom adherent
- 2 Top adherent

The bondlayer functional terms then follow by expanding:

$$\int \frac{1}{2} G_b t_b \gamma_{xz}^2 dx dy + \int \frac{1}{2} G_b t_b \gamma_{yz}^2 dx dy + \int \frac{1}{2} E_b t_b \epsilon_z^2 dx dy, \tag{25}$$

which is simply the strain energy for the bondlayer model in terms of the bondlayer strain increment components. G_b = bond shear modulus, E_b = bondlayer young's modulus and t_b = bondlayer thickness. Throughout this study these properties are assumed to be constant per bondlayer in x and y direction. Substituting equations 22 and carrying out the integrations, the result reads:

$$\begin{aligned}
F_{\text{Bond}} &= \sum_i \left\{ \phi_{B_i} (U_2^t |N| U_2 - 2 U_1^t |N| U_2 + U_1^t |N| U_1 + \right. \\
& \left. \langle \frac{1}{4} \rangle \mu \left(\frac{d_1^2}{4} W_1^t |M| W_1 + \frac{d_1 d_2}{2} W_1^t |M| W_2 + \frac{d_2^2}{4} W_2^t |M| W_2 \right) + \right. \\
& \left. \langle \frac{1}{2} \rangle \mu (d_1 U_2^t |I| W_1 + d_2 U_2^t |I| W_2 - d_1 U_1^t |I| W_1 - d_2 U_1^t |I| W_2) + \right. \\
& \left. \langle \frac{1}{3} \rangle (V_2^t |N| V_2 - 2 V_1^t |N| V_2 + V_1^t |N| V_1) + \right. \\
& \left. \langle \frac{1}{3} \rangle \frac{1}{B} \left(\frac{d_1^2}{4} W_1^t |G| W_1 + \frac{d_1 d_2}{2} W_1^t |G| W_2 + \frac{d_2^2}{4} W_2^t |G| W_2 \right) + \right. \\
& \left. \langle \frac{1}{3} \rangle \frac{1}{B_i} (d_1 V_2^t |H| W_1 + d_2 V_2^t |H| W_2 - d_1 V_1^t |H| W_1 - d_2 V_1^t |H| W_2) \right. \\
& \left. \langle \frac{1}{3} \rangle \epsilon_{B_i} (W_2^t |M| W_2 - 2 W_1^t |M| W_2 + W_1^t |M| W_1) \right\}. \tag{26}
\end{aligned}$$

$$\text{with } \phi_{B_i} = \frac{L}{4} G_{B_i} \frac{B_i}{t_{B_i}}, \quad \epsilon_{B_i} = \frac{L}{4} E_{B_i} \frac{B_i}{t_{B_i}},$$

$$d_1 = t_1 + t_b, \quad d_2 = t_2 + t_b, \quad \mu = M\pi$$

It is noted that this bondlayer finite element formulation does not require additional degrees of freedom to describe joint behavior, since only nodal amplitudes of the adherent plate elements occur in expression 26.

For the rivet-line model the following procedure is adopted. Each rivet is assumed to be a beam with circular cross section. It's deformation is expressed by three displacement modes, one stretching and two bending modes. Selecting it's nodal points to coincide with the joining flange and skin elements' midplanes, these modes are expressed in terms of the plate element displacement function amplitudes.

The rivet-line energy term is obtained by summing all rivet contributions per stringer-skin joint. Thus, with reference to fig. 6, the energy reads:

$$\Sigma \left\{ \frac{1}{2} E_{R,RO} \int_0^{L_R} (u_{R,zz})^2 dz + \frac{1}{2} E_{R,RO} \int_0^{L_R} (v_{R,zz})^2 dz + \frac{1}{2} A_{R,RO} \int_0^{L_R} (w_{R,z})^2 dz \right\} \quad (27)$$

where subscript R denotes rivet.

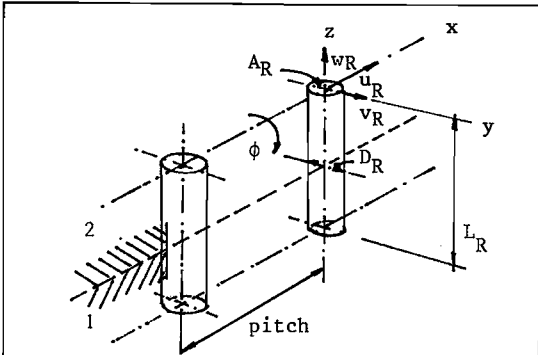


Figure 6. Rivet model
1, 2 Bottom and top joining plates.

Selecting 3-rd-degree polynomials for U_R , V_R and a linear expansion for W_R in $\xi = \frac{z}{L_R}$, as in the nature of equations 22, the pertinent matrix form of equation 27 is found. Then after expressing the U_R , V_R and W_R nodal amplitudes in the appropriate flanges or skin displacement-amplitudes, the total rivet line contribution is found after carrying out a summation over all rivets per line. The result is:

$$F_{R/line} = \frac{1}{2} \left(\begin{matrix} C_{us} \\ C_{uc} \end{matrix} \right) \mathcal{U}^T |K_{\mathcal{U}}| \mathcal{U} + \begin{matrix} C_{vs} \\ C_{vc} \end{matrix} \mathcal{V}^T |K_{\mathcal{V}}| \mathcal{V} + \begin{matrix} C_{ws} \\ C_{wc} \end{matrix} \mathcal{W}^T |F| \mathcal{W} \right) \quad (28)$$

where, $\mathcal{U}^T = (U_1 \ W_1 \ U_2 \ W_2)$
 $\mathcal{V}^T = (V_1 \ \phi_1 \ V_2 \ \phi_2)$
 $\mathcal{W}^T = (W_1 \ W_2)$

The detailed expressions are obtained in standard fashion, reported in ref. 11, and summarized in appendix I. Taking variations with respect to \mathcal{U} , \mathcal{V} and \mathcal{W} in equations (26) and (28) yields the bondlayer- and rivet-line stiffness matrices.

Method of solution

The results of the foregoing derivations are employed to generate the system of equations for the solution of the buckling problem. This procedure is performed in well-known finite element sense. As indicated above the system of equations is equipped with terms arising from the inclusion of the non-linear material law either unmodified or modified for local-buckling effects. Hence the determination of the critical load implies the necessity to solve an eigenvalue problem with highly non-linear coefficients matrices.

An efficient method for the computation of the critical load is a simple search for the sign change of the total matrix determinant, corresponding to the smallest eigenvalue. The particular small bandwidth structure of the system matrix, in particular for stiffened panel finite element models, allows the sequential decompositions for calculating the determinant as a function of the panel end-shortening, to be carried out very efficiently in view of required C.P.U. times. Earlier employed power method iteration techniques can not compete with the determinant search method.

Results and discussion

The 'Experimental Method Fokker', outlined in section II.1, as a computational tool for estimating critical loads of stiffened compression panels, has been employed for design and stressing purposes for a number of years. Correlation of the unmodified method's computational results with test data was extensively reported by Michon (12,13).

Hence, this section summarizes some of the results obtained with the modified version of the E.M.F., that allows for the buckling mode to differ from the Euler wave form. This, in the sense that any deformation component in the panel's lateral direction develops freely and is determined by solving the buckling problem contained in equation 23. The main differences between the two formulations are repeated here as:
 - panel section deformation
 - in-plane shear deformation
 - modified plasticity theory
 - flexible skin-stringer joint behavior
 and are of importance, when comparing computational results obtained herein, with the traditional version of the E.M.F. and test data.

As for the latter, any comparison with test data should be appreciated in a proper perspective. In practice, the single test result is, usually, the panel maximum load, sustained in a flat ended compression test. This load, generally, represents limit point buckling in a load end-shortening diagram. From the general theory of elastic stability (14) it is well known that the limit load is a function of the panel's initial imperfection form, as contrasted to the bifurcation load that results for the perfect mathematical model adopted in the computations. This aspect is exemplified in fig. 7.

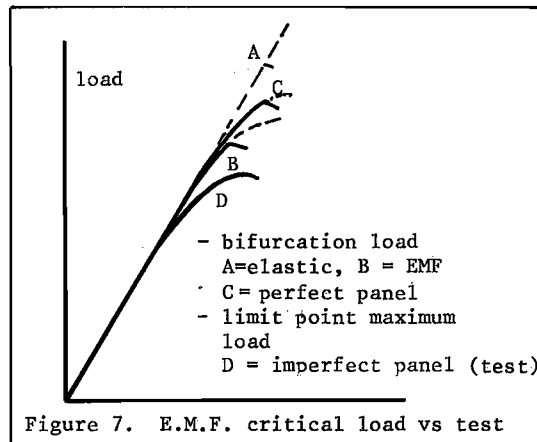


Figure 7. E.M.F. critical load vs test

In addition, the E.M.F. load is obtained on the basis of the relations 2 and 11, the coefficients of which were determined from tests. Hence, the computational results feature a statistical character, with respect to the scatter bands of the short column load end-shortening curves (ref. 6).

The first results to be presented are E.M.F. critical stresses or loads correlated with analytically or numerically obtained values. Next a selection of previously reported computational results and test data will be listed and compared with the results obtained with the modified formulations as presented in this report.

An analytical approach to the plastic plate buckling problem was recently reported by Shrivastava⁽²¹⁾. The finite element solution, obtained by the E.M.F. for square simply supported plates is compared to the findings of ref. 21 in the following table.

PAN.ID ($\frac{b}{t}$)	σ_{EMF}	$\sigma_{REF.21}$
22	60.48	60.5
24	57.78	57.5
26	54.18	54.-
28	49.27	49.2
σ in ksi		

Table 2. Plastic buckling stress for simply supported square plates.

b/t =plate width/thickness.

The same reference also gives values for the plastic critical stress of the compressed cruciform column. For a flange length-width ratio of 10, the following comparison values are found:

$\frac{b}{t}$	6	7	8	9
σ_{EMF}	63.92	61.38	57.70	50.62
$\sigma_{Ref. 21}$	63.68	61.05	57.39	49.81
σ in ksi				

Table 3. Plastic critical stress for cruciform column. (loaded edges simple support).

The E.M.F. values for the critical stresses in both cases were obtained with a 3 node-model or 2 elements per side. In the square simply supported panel case symmetry conditions are enforced, while in the cruciform example no other boundary conditions are required than the support condition, $W=0$, along the three supported edges.

In order to set the E.M.F. computed critical loads (stresses) in line with those obtained by different numerical methods, table 4 lists critical loads for a skin-stringer section.


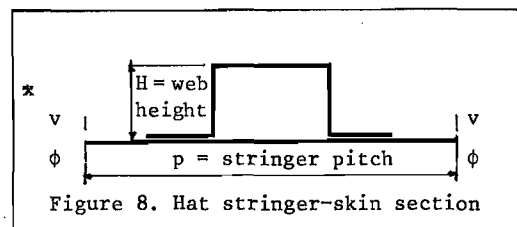
* 		
<u>Elastic analysis</u>		
t_{str}/t_{skin} 2/2,5	BUCKLASP ⁽¹⁵⁾	412.6 (N/mm ²)
	STAGS ⁽¹⁶⁾	430.2
	EMF	410.9
4/5	NASTRAN ⁽¹⁷⁾	415.7 (N/mm ²)
	EMF	395.3
1.6/1.2	BOSOR 4 ⁽¹⁸⁾	1059 (N)
	EMF	1015
<u>Plastic analysis</u>		
2/2,5	STAGS ⁽¹⁶⁾	124820 (N)
	EMF	118492

Table 4. Z-stringer-skin section

The elastic analysis performed with the E.M.F. implies no modification for local buckling and/or plasticity effects. The models employed were adapted to the specific possibilities of the comparison programs. It is noted that the higher values listed for STAGS and NASTRAN are mainly due to the coarse meshes adopted to avoid long c.p.u. times. The BOSOR4 result is obtained by utilizing the R=infinity option, offered in ref. 18, to analyze flat plates, within the context of an axi-symmetrical shell analysis formulation. A further computational comparison result is offered thru application of the STAGS-code from ref. 16 to a similar skin-stiffener section in a complete non-linear analysis. An initial imperfection, in the nature of the buckling mode is incorporated in the model, with a maximum amplitude of one half the skin thickness. In addition, the material-law for 7075-T6 al-alloy, is adopted to represent material non-linear behavior. The STAGS limit point load level is compared to the E.M.F. bifurcation load in table 4. Table 5 lists results of computations for hat-stiffener panel sections. The model consists of a single stringer and skin part as indicated in figure 8.



* v, ϕ indicate boundary conditions enforced to be zero along the longitudinal edges.

The comparison values in the table were obtained by adjusting the orthotropic material properties of an equivalent Bucklasp model⁽¹⁵⁾ to those prescribed by J2-flow theory of plasticity. The panel identification in the table is defined by the stringer pitch P and the web height H as PPPHH in mm.

Pan.ID.	Critical stress N/mm ²	
	EMF	Bucklasp
15050	449.0	451.3
14045	431.6	415.8
16055	460.5	481.7
15060	471.9	481.7
15055	461.6	476.6
13050	455.9	461.4
15045	425.3	405.7
17050	443.9	441.1
All panels L = 600 mm		

Table 5. Hat stringer skin section plastic critical stress.

The differences between the E.M.F. and Bucklasp results are mainly attributed to slight differences in structural model and material-law representation. Since the Bucklasp model has no mechanism to account for local buckling effects, the E.M.F. calculations utilize equation 2 as material-law for this case. (See note end of p. 10).

In any finite element analysis it is of interest to have an indication of the model's convergence characteristics with respect to the number of degrees of freedom that define the numerical model. The following table compares critical stresses of a Z-stringer-skin model, which is representative for a Z-stringer stiffened panel. The longitudinal edge boundary conditions imply no edge lateral displacement and no edge rotation. These conditions are enforced for the buckling displacement fields.

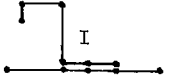
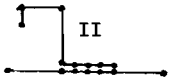

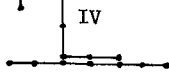
F.E. model	σ_{CR} N/mm ²
	436.05
	435.81
	434.99
	434.99
V=0 V=0 φ=0 φ=0	L = 550 mm

Table 6. Z-stringer-skin model critical stress. — nodal point (4-dofs).

It is seen from the table that the maximum difference is .36% between models I and IV. Hence, for practical computations model I would suffice in view of accuracy. Model II is included in the set for the determination of bondlayer

stresses from the buckling mode. Though the critical stresses do not show much difference, it is found that the buckling mode - normalized for maximum displacement amplitude - for model II yields higher bondlayer stresses than the modes obtained for the other models. This fact will be exemplified below.

As a comparison with previously obtained results, table 7 summarizes a selection of computed critical loads for redux bonded hat-stringered panels, taken from ref. 13.

Panel with 4 Hat stringers. Mat. Al-7178.				
PAN.ID	Test-load Comp. crit. load.			
	Present			Ref. 13
	SS	CL	SS	SS
101	1.14	1.07	1.10	1.07
104	1.20	1.19	1.18	1.19
201	1.16	1.10	1.09	1.11
204	1.12	1.08	1.17	1.17
301	1.13	1.10	1.09	1.08
304	1.12	1.11	1.10	1.13
401	1.05	1.02	1.00	1.02
404	1.05	1.03	1.06	1.12
	Extruded		Rolled	

Table 7. Redux bonded hat-stringered panels. Ref. 13.

Bond properties: $G_B/E_B/t_B = 1000/2600/.2$

Panels xx1 : L = 1100, xx4 : L = 700 mm

$t_{str}/t_{skin} : 1^{**}, 3^{**} = 2/2,5$

2**, 4xx = 3,3/2,5. (G, E N/mm²; t = mm)

SS, CL = Simple Support, Clamped Loaded edge for boundary conditions.

On account of the above noted differences between the E.M.F. procedures employed in ref. 13 and the present method, the ratios found with the finite element method should be somewhat higher than those listed in column 4 of table 7. Notably the rolled section results represent higher critical loads then computed on the basis of Euler's formula. This fact however is simply attributed to the F.E.M. model of the stiffener section corners. In general, the hat-stringered panel configurations do not require an analysis via the modified formulations.

Table 8 shows results for Z-type stiffened panels, for which test results and computations were reported by Michon⁽¹²⁾.

Computed critical loads are compared in the table with test values and those calculated with the Euler-type method.

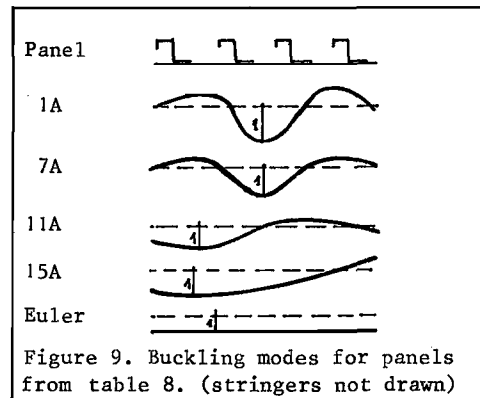


Figure 9. Buckling modes for panels from table 8. (stringers not drawn)

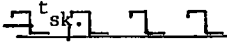
Pan. ID	t_{str}  t_{sk} Mat. 2024 al.		Critical load (kg)		Test
	t_{str}/t_{sk} (mm)	Present		Ref. 19 (TH 3)	
		SS	CL		
				SS	
1A .6/.8	1749	3358	6387	800	5750
7A 1/.8	3654	5354	7679	1100	6900
11A 1/1.4	8451	10615	11213	4300	9400
15A 1.6/1.6	13833	14086	15310	7700	13700

Table 8. Bonded Z-stringered panels, ref. 12
Fokker rep. S-118.
Bond prop. $G_B/E_B/t_B = 50/130/.2$
Loaded edge bound. cond:
SS = Simple Support
CL = Clamped Edges

It is seen that the previously obtained results overestimate the test load, reason for the recommendation in ref. 12 to apply a knock-down factor of .8 to the computed critical loads. The first column lists the critical loads computed with the F.E.M. formulation of the E.M.F. It is observed that a considerable lower load is found for the thin sheet panels, while the difference between the test value and the result in column 1 decreases with thicker sheet dimensions. The smaller sheet thickness allows for more deformation of the panel section as represented by the buckling modes. These modes are schematically drawn in figure 9.

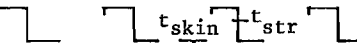
PAN. ID	t_{skin}  t_{str} Mat. 7075 al.		$\frac{N_{test}}{N_{pres.}}$	$\frac{N_{test}}{N_{TH.3} (19)}$	$\frac{N_{test}}{N_{Euler}}$
	t_{str}/t_{skin}				
PL-16 FM	2.3 2.5		1.02	.79	.78
PL-21 EC			.92	.80	.72
PL-25 FM	3.4 4.1		1.01	.93	.74
PL-26 FM			1.01	.80	.80
PL-31 EC	4		.78	.62	.62
PL-36 FM	5		1.01	.82	.81

Table 9. Test load/computed load bonded Z-stringered panels. Loaded edges simple support. L = 1400 mm.

Column 5 in table 8 shows the local buckling loads as derived from strain gauge measurements performed during the tests (ref. 12). It thus follows that the thinner panels exhibit a stringer-skin buckling point in the load end-shortening curve which does not precipitate immediate collapse. Perusing the strain gauge measurements and load-shortening curve for panel 7A for instance, one may conclude that at a load level of 4000 kg stringer rotation occurs which is indicative for the buckling mode depicted in fig. 9. Hence the modified formulation does identify such critical points. However, failure takes place at a load of 6900 kg. Since the failure mode apparently contains part of the buckling mode shown, which is not represented in the Euler type approach, persistent overestimation is found with the computational method as utilized in ref. 12.

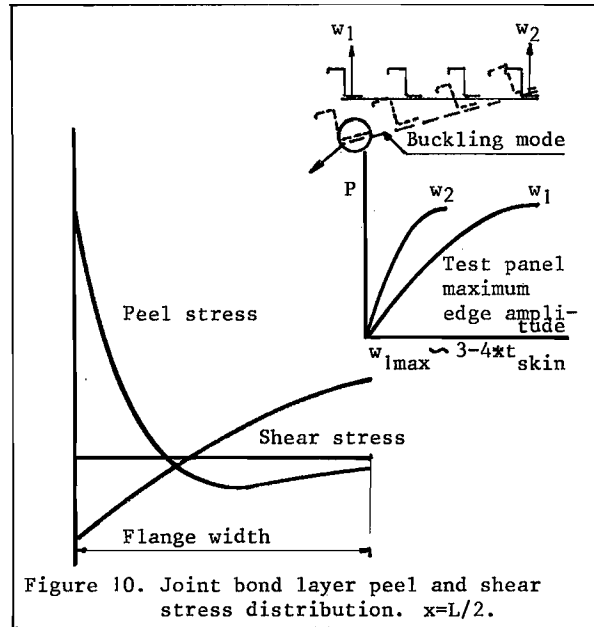


Figure 10. Joint bond layer peel and shear stress distribution. $x=L/2$.

The results given for panel 15A in table 8 and the buckling mode, depicted in fig. 9, show better correspondence with the failure load and collapse mode, which furnishes better agreement between theory and test.

The latter notion is corroborated by results of a series of recently obtained test values for Z-stiffened panels. Table 9 shows the ratio of test load and computed critical load for long, bonded panels. The buckling mode found for all geometries corresponds to the failure mode. It is shown in figure 10.

The notation FM and EC in the table indicates bond material properties as:
FM = FM-123/5: $G_B/E_B = 50/130$, EC = EC-2216:
 $G_B/E_B = 5/13$.
These values apply for the results of table 9.

The last column in the table indicates the circumstance that for these panels the deformation of the cross-section is the main reason for the Euler type approach to overestimate the test-value. The lower values of the N_{test}/N_{comp} ratio

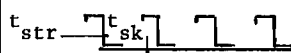
 Mat. al 7075			
Pan.ID (t_{str}/t_{sk})	Test load Comp.crit. load		$\frac{N_{rivet}}{N_{bond}}$
	Rivet	Bond	
1 (2/2.5)	1.23	1.05/1.13	.86
2 (3.2/4)	1.08	.91/.98	.93
3 (4/5)	1.05	.93/1.0	.92
4 (4/3)	1.11	.89/.95	.95

Table 10. Test load vs calculated critical load for nominally equal bonded and riveted Z-stringered panels.

All panels: $L = 1100$ mm, $\text{reduc } 775$,
bonded panels: $G_B, E_B = 50-130/10-26$

for panels, bonded with EC 2216, is attributed to the selected values of G_B and E_B , which are too high. The choice of specific values for the bond-material properties is still somewhat arbitrary. It is known that the shear modulus for many bond-materials does not attain it's torsion-pendulum value, in actual structural applications. For instance, the shear modulus found in thick adherent lapjoint tests is on average 75% the T.P. value. See ref. 20. Young's moduli are generally unknown.

The above noted deformation of the panel cross-section - a significant departure from the simple Euler buckling mode - has additional consequences for the maximum load of bonded Z-stringered panels. The unsymmetry of the stiffener - the main reason for reducing the Euler load - induces a complex stress distribution in the bondlayer. Fig. 10 shows the peel- and shear stress distribution in the bondlayer, derived from the panel's buckling mode.

In addition, the test panel configuration, with free unloaded longitudinal edges and having small width, shows considerable rotation at lower load levels. Load-edge-displacement curves indicate a beam-column type behavior, which is non-uniform in panel lateral direction. This phenomenon is depicted in fig. 10.

Hence, high bond stress levels may be expected in the test, before the maximum load is reached. Correlating panel edge deflections with the buckling mode provides an estimate for the maximum bondlayer stresses. This then indicates the bondlayer material to enter the plastic part of the material's stress-strain curve. Hence, since these curves show almost perfectly plastic behavior, local debonding is likely to occur at pre-collapse load levels.

Table 10 summarizes test results as correlated with computed critical load values for, nominally identical, bonded and riveted compression panels.

The last column in table 11 shows the better performance of the bonded panels.

Conclusion

A formulation is presented for the computation of critical loads of stringer stiffened panels in axial compression. The specific features of the E.M.F., to account for stiffness reduction as arise from local buckling and plasticity effects, has been outlined. Results of the finite strip formulation, proposed herein, are compared with analytically and numerically obtained solutions and correlated with test data. It has been shown that the E.M.F. computes reasonable estimates for failure loads of stringer stiffened panels in compression, in cases where no critical points occur between the local buckling load and the collapse load. The traditional E.M.F. (ref. 19), assuming no panel section deformation, can still be employed for computation in cases where the failure mode does not significantly depart from from the Euler mode, e.g. hat-stringered panels. The modified E.M.F. may underestimate the failure load considerably if the panel exhibits pre-failure buckling modes. It would appear recommendable to extend the capabilities of the E.M.F. with procedures to determine the stability characteristics of the panel at such critical points.

Acknowledgement

All results quoted as obtained by the STAGS and BUCKLASP programs were made available by Dr. E. Riks of the National Aerospace Laboratories, N.O.P., the Netherlands, which is gratefully appreciated.

APPENDIX I Matrices, occurring in equations 23, 26

$$\begin{aligned} |N| &= \frac{1}{6} \begin{vmatrix} 2 & 1 \\ 1 & 2 \end{vmatrix} \\ |F| &= \begin{vmatrix} 1 & -1 \\ -1 & 1 \end{vmatrix} \\ |D| &= \frac{1}{2} \begin{vmatrix} -1 & -1 \\ 1 & 1 \end{vmatrix} \end{aligned}$$

$$\begin{aligned} |M| &= \frac{1}{35} \begin{vmatrix} 13 & -11/6 & 9/2 & 13/12 \\ & 1/3 & -13/12 & -1/4 \\ & \text{sym.} & 13 & 11/6 \\ & & & 1/3 \end{vmatrix} \\ |L| &= \begin{vmatrix} -6/5 & 11/10 & 6/5 & 1/10 \\ 1/10 & -2/15 & -1/10 & 1/30 \\ 6/5 & -1/10 & -6/5 & -11/10 \\ 1/10 & 1/30 & -1/10 & -2/15 \end{vmatrix} \end{aligned}$$

$$|K| = \begin{vmatrix} 12 & -6 & -12 & -6 \\ & 4 & 6 & 2 \\ & \text{sym.} & 12 & 6 \\ & & & 4 \end{vmatrix}$$

$$|G| = \frac{1}{30} \begin{vmatrix} 36 & -3 & -36 & -3 \\ & 4 & 3 & -1 \\ & \text{sym} & 36 & 3 \\ & & & 4 \end{vmatrix}$$

$$|I| = \begin{vmatrix} 7/20 & -1/20 & 3/10 & 1/30 \\ 3/10 & -1/30 & 7/20 & 1/20 \end{vmatrix}$$

$$|H| = \begin{vmatrix} -1/2 & -1/12 & 1/2 & 1/2 \\ -1/2 & 1/12 & 1/2 & -1/12 \end{vmatrix}$$

Rivet line model

The coefficients in equation 28 are:

$$C_{u_s} = \frac{EI_R}{L_R^3} C_o \quad C_{u_c} = \frac{EI}{L_R^3} S_{cl_1}$$

$$C_{v_s} = \frac{EI_R}{L_R^3} \cdot S_i \quad C_{v_c} = \frac{EI_R}{L_R^3} S_{cl_2}$$

$$C_{w_s} = \frac{EA_R}{L_R} \cdot S_i \quad C_{w_c} = \frac{EA_R}{L_R} S_{cl_2}$$

Where, with N_R = number of rivets/line and P_R = rivet pitch, $\mu = M\pi/L$ and M = wavenumber:

$$C_o = N_R/2 + \frac{1}{2} \frac{\text{SIN}(N_R \cdot \mu \cdot P_R)}{\text{SIN}(\mu \cdot P_R)} * (-1)^M$$

$$S_i = N_R/2 - \frac{1}{2} \frac{\text{SIN}(N_R \cdot \mu \cdot P_R)}{\text{SIN}(\mu \cdot P_R)} * (-1)^M$$

$$S_{cl_1} = N_R/2 - \frac{1}{2} \frac{\text{SIN}(N_R \cdot 2\pi P_R/L)}{\text{SIN}(2\pi P_R/L)}$$

$$S_{cl_2} = N_R + 2 \frac{\text{SIN}(N_R \pi P_R/L)}{\text{SIN}(\pi P_R/L)}$$

In addition:

$$\begin{aligned} |K_u| &= |TR_u| |K| |TR_u| \\ |K_v| &= |TR_v| |K| |TR_v| \end{aligned}$$

where

$$|TR_u| = \begin{vmatrix} 1 & & & \\ & \mu \cdot L_R & \bigcirc & \\ & & 1 & \\ \bigcirc & & & \mu L_R \end{vmatrix} \text{ and } |TR_v| = \begin{vmatrix} 1 & & & \\ & -L_R & \bigcirc & \\ & & 1 & \\ \bigcirc & & & -L_R \end{vmatrix}$$

(ref. fig. 6).

- 1 G.J. Fonk.
The influence of local buckling on the primary failure of stiffened panels, loaded in compression.
Proc. 2nd Eur.Aeron.Congress.
Scheveningen, The Netherlands, Sep. '56
- 2 M.S. Cheung, M.Y.T. Chan.
Three-dimensional finite strip analysis of elastic solids.
Comp. & Struct. vol. 9, pp. 629-638. 1978
- 3 M. Botman.
Het draagvermogen van panelen.
N.L.R. rapport S-463, 1956 (in Dutch).
- 4 F.R. Shanley.
Strength of materials.
McGraw-Hill Book cy. N.Y., 1957.
- 5 Bruce G. Johnston (ed.)
Guide to stability design criteria for metal structures. 3rd ed.
Wiley-Interscience N.Y., 1976.
- 6 A.W. Spaink.
Examination of the procedures used at Fokker for calculating compressive loads of short sections.
Fokker report S-139, 1976.

- 7 W. Ramberg, W. Osgood.
Description of stress-strain curves by three parameters.
NACA-TN.901. 1943
- 8 E.Z. Stowell.
A unified theory of plastic buckling of plates and shells.
Journ.Aeron.Sciences. Sep.'49, pp. 529-541.
- 10 H. Durlowsky, J. Mayers.
Effects of interlaminar shear on the bending and buckling of laminated beams.
USAAVLABS-TR-70-7. 1970.
- 11 J.H. van der Sloot.
The riveted stringer option in the modified E.M.F. computer analysis.
Fokker report SM-108. May 1979.
- 12 A.C.W. Michon.
Theoretical and tested compressive strength of flat panels in 2024 aluminum alloy.
Fokker report S-118. 1966.
- 13 A.C.W. Michon.
Theoretical and experimental compressive strength of flat bonded panels with 7075 and 7178 aluminum alloy skin, stiffened with 7178 aluminum alloy hat section stringers.
Fokker report S-122. Sep. 1966.
- 14 W.T. Koiter.
The stability of elastic equilibrium.
AFFDL-TR-70-25. Feb. 1970.
- 15 A.V. Viswanathan, Tsai Chen Soong, R.E. Miller jr.
Buckling analyses for axially compressed flat plates, structural sections, and stiffened plates reinforced with laminated composites.
NASA-CR-1887. Wash.D.C. Nov. 1971.
- 16 B.O. Almroth, F.A. Brogan, M.B. Marlowe.
Collapse analysis for shells of general shape. Vol.I. Tech.rep. AFFDL-71-8. Aug. 1972.
- 17 L. Peterson (ed.).
MSC/NASTRAN. MSGMESH analyst's guide.
The Macneal-Schwendler Corporation, Los Angeles, CA. Apr. 1978.
- 18 D. Bushnell.
Stress, stability and vibration of complex branched shells of revolution: analysis and user's manual for BOSOR4.
NACA-CR-2116. Oct. 1972.
- 19 Fokker Stress Manual TH 3.
- 20 W. Althof, et.al.
Klima Einfluss auf die Kennwerte des elasto-plastischen Verhaltens von Klebstoffen in Metallklebungen;
DFVLR-Braunschweig DLR-FB 77-63. 1978.
- 21 S.C. Shrivastava.
In-elastic buckling of plates including shear effects.
J. of Solids and Structures. Vol. 15 pp. 567-575. 1979
- 22 K. Washizu.
Variational methods in elasticity and plasticity.
Pergamon Press. 1st ed. 1968.
- 23 J.W. Hutchinson.
Plastic buckling.
In 'Advances in applied mechanics'. Vol. 14. 1974.